The Journal of the Korean Institute of Electrical and Electronic Material Engineers. Vol. 9, No. 4, pp.385-395,1996.

금속성 이물질에 의한 불평등전계중에서 SF_6가스의 절연특성과 방전현상

논 문
9-4-8

Dielectric Behaviors and Discharge Phenomena of SF_6 Gas in Inhomogeneous Field Caused by a Conducting-particle

이복희*, 안창환*, 이창준*, 길경석**, 전덕규***, 백승권$
(Bok-Hee Lee*, Chang-hwan Ahn*, Chang-Jun Lee, Gyung-Suk Kil**,
Duk-Kyu Jeon***, Seung-Kwon Paek$)

요 약

이 논문은 금속성 돌기물에 의한 불평등전계중에서의 비진동성과 진동성 임펄스전압에 의한 SF_6 가스의 절연파괴 특성에 대해 기술하였다. 절연파괴전압-시간특성을 가스압 0.1-0.5 MPa의 범위에서 정·부극성의 전압을 인가하여 측정하였으며, 그리고 50Ω 분류기를 통해서 전구방전전류를 관측하였다. 가스압력에 의한 리이더 진전시간의 의존성도 측정하였다. 스트리머 코로나에 의해 발생하는 공간전하에 의한 국부전계강화는 시험갭의 전기적 절연파괴에 영향을 미치는 것으로 판명되었다. 절연파괴는 초기 스트리머 코로나로부터 발단되어, 국부전계강화에 의한 리이더진전으로 이루어진다.

Key Words(중요용어) : SF_6 Gas(SF_6가스), Gas-Insulated Switchgear(가스절연개폐장치), Fast Transient Overvoltages(과도파전압), Prebreakdown Phenomena(전구방전현상), V-t Characteristics(V-t특성), Leader mechanism(리이더 기구), Streamer Corona(스트리머 코로나)

1. Introduction

The sulphur-hexafluoride(SF_6) is a gas of widespread use as the insulating and quenching mediums in high-voltage equipments, because of its high dielectric strength and excellent heat transfer properties. However, strikes that occur as a result of the disconnect operation of a capacitive load lead to fast transient overvoltages(FTOs) inside the SF_6 gas-insulated switchgear(GIS). These FTOs act as travelling surges originating from the disconnecting switch and have oscillation frequencies up to more than 100 MHz.

The dielectric strength of SF_6 gas stressed by FTOs is very sensitive to the local electric field disturbed by the surface roughness of conductors or conducting-particles. Paschen's law is not generally valid in inhomogeneous field configurations, the anomalies arising from space charge effects are observed. Up to now, numerous experimental and theoretical investigations have been carried out on the dielectric breakdown behaviors of SF_6 gas for quasi-uniform electric fields and D.C or well-defined voltages. In particular, in order to improve the reliability of GIS, the understanding of the discharge phenomena of SF_6 gas and the detailed study for the influences of conducting particles on the discharge development are of great important[1-5].

Further works of the discharge phenomena of SF_6 gap stressed by fast transient overvoltages in inhomogeneous field caused by the conducting-particles need to be investigated. The purpose of this work is to present informations on the prebreakdown phenomena of the conducting-particle-initiated breakdown for the sake of the insulation and coordination in GIS. The experiments have been performed by using non-oscillating and damped-oscillating impulse voltages in the simplified coaxial cylindrical electrode arrangements.

The experimental apparatus was made of a

* : 인하대학교 전기공학과
** : 한국해양대 이공대 전기공학과
*** : 서울산업대 공대 전기공학과
$: 인제대 공대 전기공학과
접수일자 : 1995년 9월 4일
심사완료 : 1996년 2월 20일

400 kV real-sized GIS arrangement. The breakdown voltage-time characteristics and prebreakdown developments for positive and negative polarities were measured. All signals were recorded by a transient digitizer with a bandwidth of 350 MHz. The electrical breakdown is caused by a conducting-particle and the influence of the oscillation frequency on the prebreakdown development processes is significantly presented. In addition, the prebreakdown behaviors are discussed in detail based on the waveform of corona current pulses.

2. Measuring Principle of Prebreakdown Current

The conductivity of gas is originated from the fact that charged particles such as electrons or ions exist in the gas, and an electric field moves the charged particles, so the current flows in the gas. When the discharge takes place in the gap, the prebreakdown current results from the moving space charge except the outside element.

In Fig. 1, the current I_i in the ith electrode due to the point charge q at free position r can be expressed as

$$I_i = \frac{q\mathbb{V}(r) \cdot \mathbb{E}_{0i}(r)}{V_i} \tag{1}$$

where $\mathbb{E}_{0i}(r)$ is the electric field at ith electrode, $\mathbb{V}(r)$ is the velocity of q at r, and V_i is the potential at ith electrode.

In the following, we will use Poynting vector to derive an expression for the electrode lead current[6,7]. The input power in the electrode system is given by Poynting vector.

$$P_{in} = -\int\int_S (\mathbb{E}\times\mathbb{H}) \cdot d\mathbb{S} \tag{2}$$

where $\mathbb{S}$ is a closed surface made up partly by the electrode surface and also by another surface chosen sufficiently far away that the plasma contribution to $\mathbb{E}$ at that surface is negligible.

The electric field $\mathbb{E}$ is assumed to be brought about by superposition of two different electric fields: the space charge free field between the

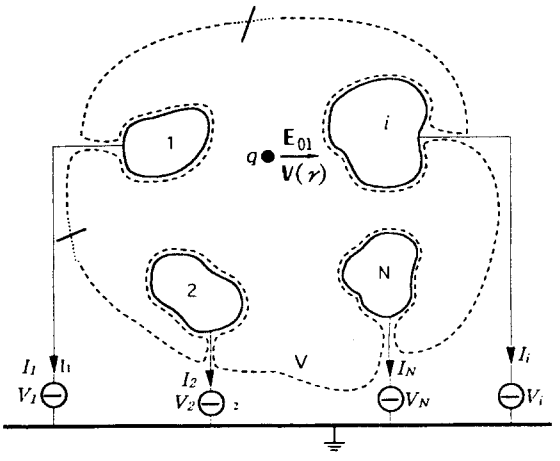

그림 1. 공간전하가 존재하는 경우의 다전극계
Fig. 1. Mult-electrode system with space charge inside the inter-electrode volume

electrodes $\mathbb{E}_0$ and the electric field $\mathbb{E}_{SC}$ due to the free space charges. The input power can now be rewritten as

$$P_{in} = \int\int\int_v \mathbb{E}_0 \cdot \mathbb{J} dv + \int\int\int_v \mathbb{E}_{SC} \cdot \mathbb{J} dv$$

$$+\varepsilon_0 \int\int\int_v \mathbb{E} \cdot \frac{\partial \mathbb{E}_{SC}}{\partial t} dv + \varepsilon_0 \int\int\int_v \mathbb{E} \cdot \frac{\partial \mathbb{E}_0}{\partial t} dv \tag{3}$$

where v is a volume made up by the closed surface $\mathbb{S}$. Using Gauss' theorem and continuity equation, the input power is given as following;

$$P_{in} = \int\int\int_v \sum(\mathbb{E}_{0i}) \cdot \mathbb{J} dv$$

$$+\frac{1}{2}\frac{\partial}{\partial t}\varepsilon_0 \int\int\int_v \sum(\mathbb{E}_{0i}) \cdot \sum(\mathbb{E}_{0i}) dv \tag{4}$$

Provided that the assumptions are satisfied as followings;

(1) the total electric field in the gap being curl free.

(2) the space charge electric field being curl free.

The current of a two-electrode system with one electrode grounded can be expressed as

$$I(t) = \frac{1}{V_g(t)} \int\int\int_v \mathbb{E}_{01} \cdot \mathbb{J} dv$$

$$+\frac{1}{V_g(t)}\frac{\partial}{\partial t}\frac{1}{2}\varepsilon_0 \int\int\int_v \mathbb{E}_{01} \cdot \mathbb{E}_{01} dv \tag{5}$$

where V_g is the potential difference across the

gap.

The first term on the right-hand side in Eq. (5) represents the conduction current caused by the moving space charges. The second term on the right-hand side in Eq. (5) represents the change of the electric field energy stored in the electrode system, i.e., this term stands for the displacement current component and can be written as

$$\frac{1}{V_g(t)} \frac{\partial}{\partial t} \frac{1}{2} \varepsilon_0 \int \int \int_v \mathbb{E}_{01} \cdot \mathbb{E}_{01} dv$$

$$= C \frac{\partial V_g(t)}{\partial t} \tag{6}$$

Therefore, in order to detect only the conduction current originating from the moving space charges flowing into the external circuit, it is necessary to minimize the displacement current component.

3. Experimental Apparatus and Procedure

3.1. Experimental apparatus and measuring system

The experimental apparatus used here was designed to simulate the fast transient over-voltages that might be generated in GIS during the switching operation of disconnector, and was fabricated by real-sized GIS arrangement. Fig. 2 shows a simplified diagram of the experimental apparatus. Also, Fig. 3 presents the block diagram of the total experimental system. The voltage applied to the test gap was measured by a conical type electric field probe[8]. The test voltages were non-oscillating impulse of 1.7/44μs and damped-oscillating impulse voltage of 400 ns/1.14 MHz.

A pair of coaxial cylindrical electrodes was mounted in the pressure vessel and the gap separation was 37 mm. The electric field of test gap was disturbed by a stainless steel needle-shaped protrusion on the earthside electrode. In order to minimize the displacement current as described Sec. 2, the needle-shaped protrusion was electrically isolated from the earthed electrode. Curvature radius and length of the needle-shaped protrusion are 0.3 mm, 15 mm, respectively. Thus the distance between the inner electrode and the tip of needle-shaped protrusion is 22 mm. The prebreakdown current was observed by a shunt of 50 Ω. All signals were recorded by an oscilloscope with a bandwidth of 350 MHz(Tek. 2440). The pressure vessel was evacuated to 0.13 Pa and then commercial grade SF_6 gas was filled.

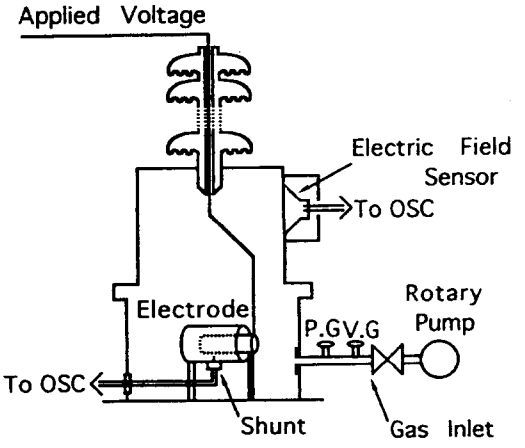

그림 2. 실험장치의 개략도

Fig. 2. Simplified diagram of the experimental apparatus

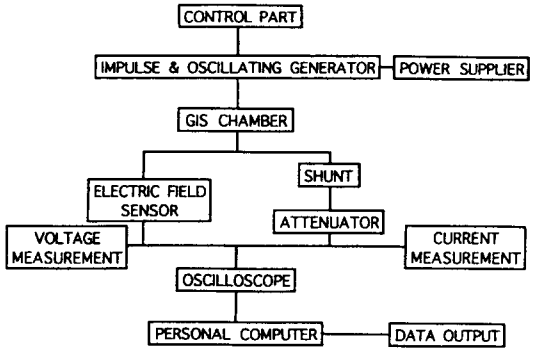

그림 3. 실험계의 블록도

Fig. 3. Block diagram of the total experimental system

3.2 Electrode geometry

Fig. 4 shows the cross-sectional view of the coaxial cylindrical electrode geometry. The outer and inner cylinder radii are 54 mm and 17 mm, respectively. To reproduce the inhomogeneous electrical field, a metallic needle-shape protrusion

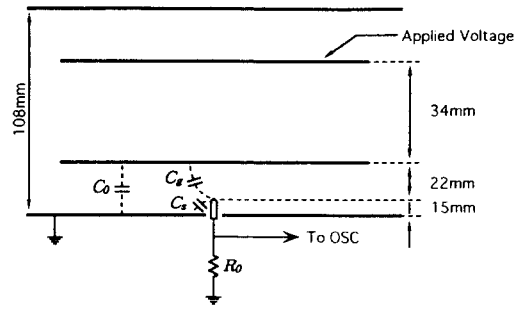

그림 4. 동축원통 전극계의 단면도
Fig. 4. Cross-sectional view of the coaxial cylindrical electrode geometry

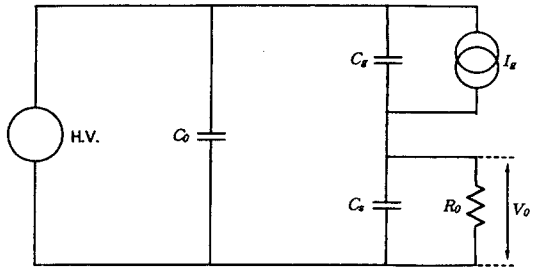

그림 5. 전극계의 전기적 등가회로
Fig. 5. Electrical equivalent circuit of the electrode geometry.

is installed at the outer cylindrical electrode. Based on the stray capacitance and the current detecting resistance, the electrical equivalent circuit for the electrode geometry can be constructed as shown in Fig. 5.

The output voltage V_0 detected by resistance R_0 is given by

$$V_0 = -\frac{R_0 I_g}{1+\frac{C_g}{C_s}+jwR_0(C_s+C_g+\frac{C_sC_g}{C_0})} \quad (7)$$

In order that the conduction current I_g is directly proportional to the output voltage V_0, the electrode system should be designed and prepared by the following conditions,

$$C_s \gg C_g,\ wR_0(C_s+C_g+\frac{C_sC_g}{C_0}) \ll 1$$

When we detect the prebreakdown current, the needle-shaped protrusion is electrically insulated from the outer cylindrical electrode so that the displacement current can be minimized. This gap geometry provides a distinct outburst of the first streamer corona and allows the measurement of the prebreakdown current minimizing the displacement current.

3.3 Electrical field distribution of the electrode system

To calculate the electrical field distribution of the electrode system, we must combine the electric fields for a coaxial cylindrical electrode and needle-to-plane electrode geometries. The electrical field of coaxial cylindrical electrode is expressed as[9]

$$E(r) = \frac{V}{r\ln(\frac{R_2}{R_1})} \quad (8)$$

where r : radius direction distance from inner cylinder

R_2 : radius of outer cylinder

R_1 : radius of inner cylinder

V : applied voltage

Also, the electrical field of needle-to-plane electrode system is given by[10]

$$E(x) = \frac{V}{A\sqrt{d(R+d)}\,(1-\frac{x^2}{d(R+d)})} \quad (9)$$

where $A = \ln(\frac{\sqrt{R+d}+\sqrt{R}+\sqrt{d}}{\sqrt{R+d}+\sqrt{R}-\sqrt{d}})$

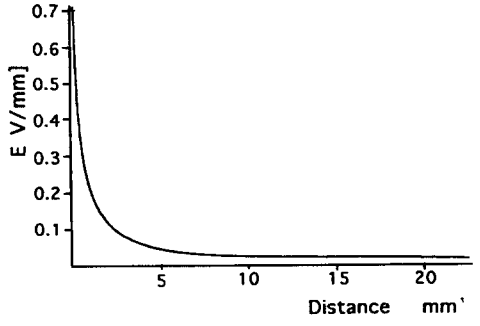

그림 6. 전극계의 규격화된 전계분포
Fig. 6. Normalized electric field distribution of the electrode system

V : applied voltage
R : curvature radius of needle
d : gap separation
x : distance from needle tip along its axis

R and d of this electrode geometry are 0.3 mm and 22 mm, respectively. Fig. 6 shows the normalized electric field distribution of the electrode system used in this work when applied voltage is 1 V.

4. Experimental Results and Discussion

4.1 Dielectric characteristics

The breakdown voltage-time(V-t) characteristics were measured by using the positive and negative non-oscillating and oscillating impulse

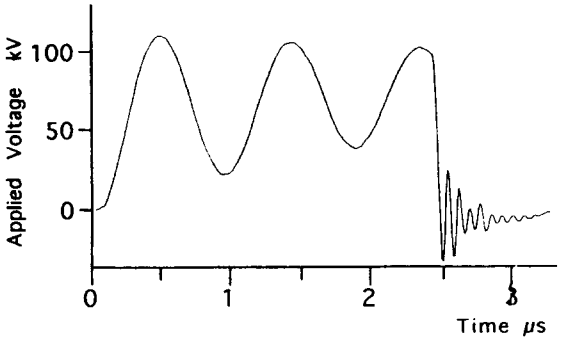

그림 7. 진동성 임펄스전압의 대표적인 파형
Fig. 7. A typical voltage waveform of the electrical breakdown for the oscillating impulse voltage

voltages. Fig. 7 shows a typical voltage waveform of electrical breakdown for the oscillating impulse voltages. The oscillation frequency and the decay time to half amplitude are 1.14 MHz and 40 μs, respectively.

Fig. 8 presents the V-t curves depending on the waveform of applied voltage for the positive and negative polarities. The V-t curves were depicted by taking the maximum voltage recorded prior to electrical breakdown, according to IEC standard 60.2. Also, the polarity of the voltage in this paper indicates on the basis of that of the needle-shaped protrusion. Also, Fig. 9 shows the examples of the breakdown points

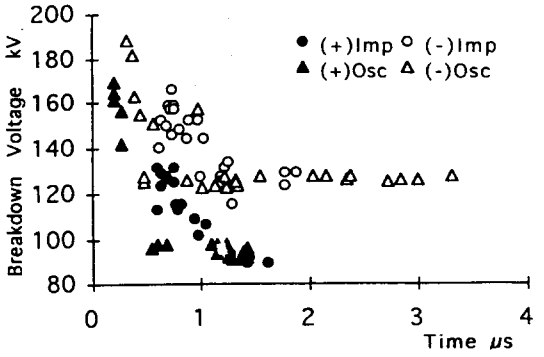

(a) P = 0.1 MPa

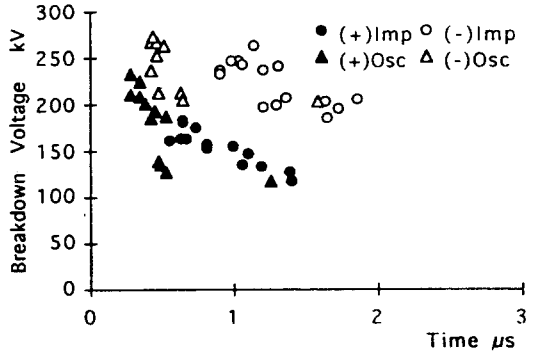

(b) P = 0.4 MPa

그림 8. 인가전압의 극성과 파형을 파라메터로 나타낸 V-t곡선
Fig. 8. V-t curves depicted as a parameter of the applied voltage waveform and polarity

for non-oscillating and oscillating impulse voltages in the positive and negative polarities. The electrical breakdown mostly occurs at the rising parts of oscillation and/or around the crests. The breakdown voltages of the negative polarity are higher than ones of the positive polarity, and the difference between the positive and negative breakdown voltages is prominent. Even in case of the same polarity the breakdown voltages for oscillating impulse voltage are almost equal to those for non-oscillating impulse voltage, but the scatter of the breakdown voltage for the negative oscillating impulse is remarkable.

The time to breakdown in the positive polarity is on the whole shorter than that in the negative polarity. The trend is noticeable for

lower gas pressure and is attributed to a leader breakdown controlled by space charges due to the streamer corona. The prebreakdown developments strongly depend on the applied voltage waveform, which affects the leader propagation across the test gap. In particular, in the presence of the negative polarity the time to breakdown of oscillating impulse voltage is noticeably longer than that of non-oscillating impulse voltage. Also, the time-lag of electrical breakdown on the wave tail is mainly subject to the field stabilization due to streamer corona space charges[11]. An electrical breakdown at the falling part of wave tail and/or trough part of oscillation can only take place if the leader overcomes the reduction of electric field caused by the variation of the applied voltage and space charges. The prebreakdown development is interrupted as the electric field strength is decreased by an oscillation of applied voltage. The consequence brings on a long time-lag between the leader steps. However, the prebreakdown development for non-oscillating impulse voltage is continuous and leads to an electrical breakdown in the short time.

In addition, in case of the oscillating impulse voltage the displacement current, which is due to the derivative of applied voltage and the capacitance between the leader tip and the opposite electrode, flows through the leader channel. This displacement current is decisive for the leader development and the subsequent breakdown. Generally, the event will act simultaneously but its weight is different

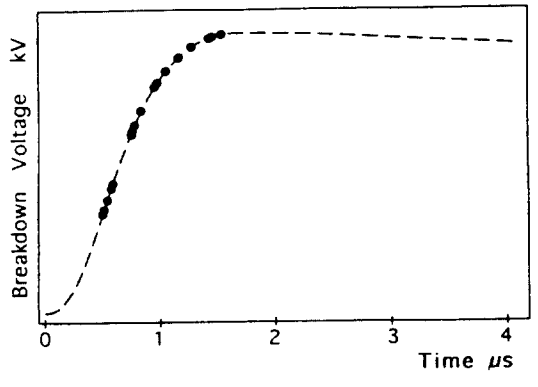

(a) Positive

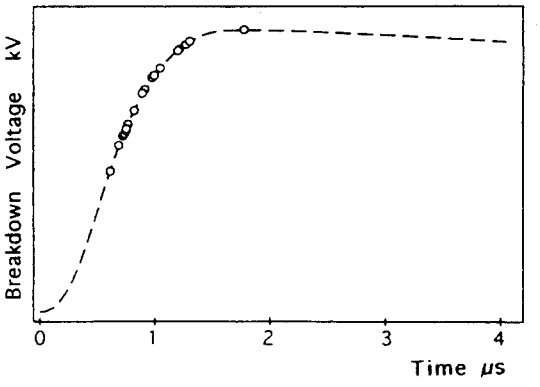

(b) Negative

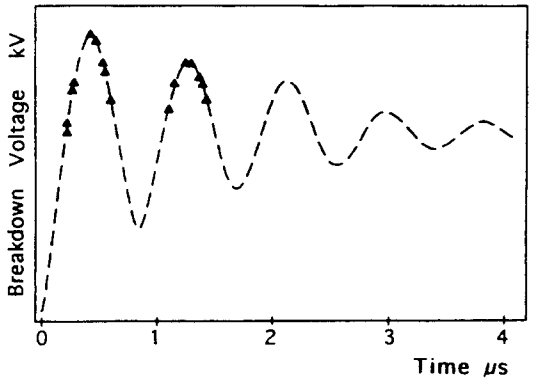

(c) Positive

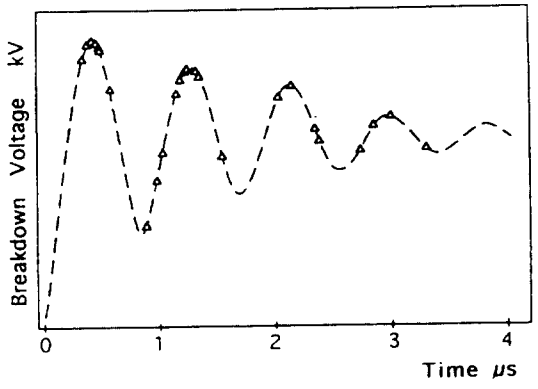

(d) Negative

그림 9. 0.1 MPa의 가스압력에서 절연파괴점의 예
Fig. 9. Examples of the breakdown points for a gas pressure of 0.1 MPa

according to the experimental conditions such as voltage waveform, gap geometry, gas pressure, polarity, and so forth. As an example, B. Heer and A. Stepken reported that the breakdown was observed only at the rising part and/or

around crests of applied voltage, and no breakdown took place near trough of oscillation[12]. Further, in order to understand the dependence of the V-t characteristics on the polarity of applied voltage, it is necessary now to consider the physical mechanism of prebreakdown developments, and the detailed behavior of the prebreakdown process should be investigated and will be discussed in Sec. 4.2.

4.2 Prebreakdown Phenomena

Fig. 10 shows the applied voltage and prebreakdown current waveforms in the positive and negative non-oscillating impulse voltages for a gas pressure of 0.2 MPa. Also the prebreakdown developments mainly depend on the gas pressure and the applied voltage

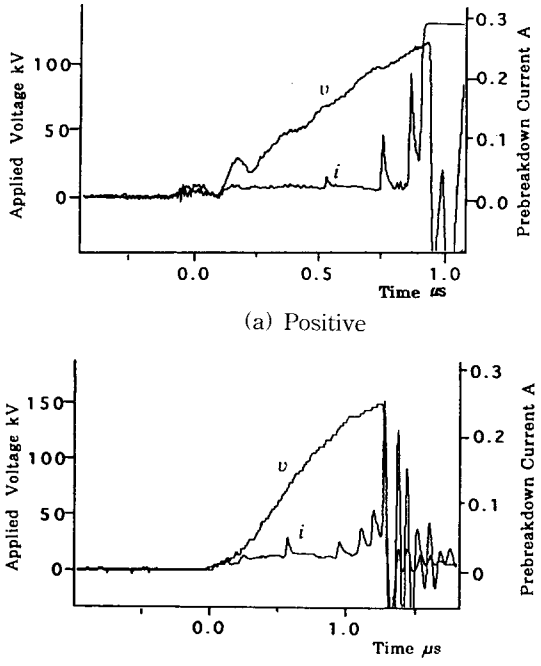

(a) Positive

(b) Negative

그림 10. 비진동성 임펄스전압에 대한 인가전압과 전구방전전류의 파형

Fig. 10. Applied voltage and prebreakdown current waveforms for non-oscillating impulse voltages.

waveform. A prebreakdown development is initiated by the first streamer corona from the tip of a needle-shaped protrusion and is propagated by a stepwise leader regime. The first streamer corona for lower gas pressure was started by a pronounced pulselike current, and it was gradually decreased with increasing the gas pressure.

Also the weakly conductive plasma channel then is formed by streamer corona in front of the needle-shaped protrusion at which the electric field becomes quasi-uniform. The streamer to leader transition for higher gas pressure is formed and the leader propagates with stepwise into the gap. The electrical breakdown takes place as the leader jumps across the gas gap. That is, it is inferred that the breakdown would take place by streamer corona sequences at the tip of the conductive plasma channel. Also, even if an applied voltage is not enough for electrical breakdown, one or more corona outbursts occur but fail to reach the opposite electrode.

There is no essential difference between the prebreakdown development mechanisms for the positive and negative polarities, but the first streamer corona current for the negative polarity was more pronounced compared to that for the positive polarity. The prebreakdown current increases with streamer corona order. Also the mean time interval between the leader steps is longer than that for the positive polarity. In the presence of the negative polarity the high current of first streamer corona and the long leader stepping time are originated from the production process of initial electrons and the distribution and lifetime of space charges due to the streamer corona.

Fig. 11 shows the voltage and prebreakdown current waveforms for the positive and negative oscillating impulse voltages. Comparing breakdown voltages between the data for the non-oscillating and oscillating impulse voltages, there is little difference as discussed in Sec. 4.1, but the different regimes of the prebreakdown developments were observed.

The prebreakdown currents in the positive polarity are bipolar corresponding to the oscillation of applied voltage. Similar observations of the correlated photographic and streamer

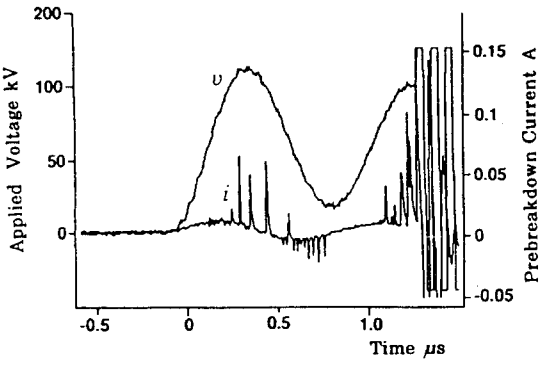

(a) Positive

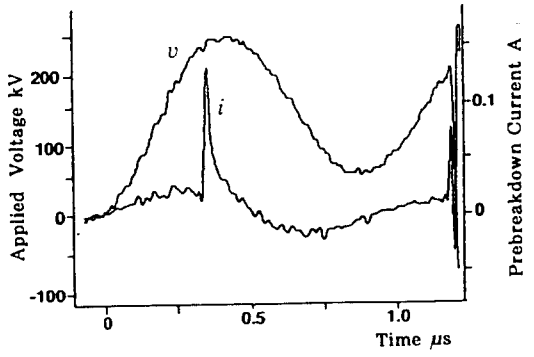

(b) Negative

그림 11. 0.2 MPa의 가스압력에서 정·부 진동성 임펄스에 대한 인가전압과 전구방전전류의 파형

Fig. 11. Applied voltage and prebreakdown current waveforms in the positive and negative oscillating impulse voltages for a gas pressure of 0.2 MPa

corona current data for the prebreakdown developments were reported by S. Matsumoto et al.[13]. The first corona at the rising part of applied voltage takes place in front of the needle-shaped protrusion and forms positive ion space charges. The positive leader then propagates with stepwise toward the opposite electrode. As the potential of the needle-shaped protrusion is decreased by the oscillation of applied voltage, there exists the potential difference between the needle-shaped protrusion and the positive space charges. This process reforms an electric field in the direction opposite to the leader development, and then the negative pulselike current flows. The implication is that the backward prebreakdown processes develop toward the needle-shaped protrusion.

If the variation rate of applied voltage is slower than the diffusing time of positive space charges, the unidirectional prebreakdown current flows. The diffusing time of positive space charges determines whether a bipolar current flows or not. The bipolar prebreakdown current is mainly related to the oscillation frequency of applied voltage, gas pressure and gap geometry.

The negative prebreakdown development is started by the first streamer corona, which is a very small at the front part of oscillation wave. The prebreakdown development pattern is essentially similar to the positive prebreakdown current waveform. The accompanying current pulse is extremely larger than that of the first corona current. But after the appearance of strong corona current pulse, the leader is stopped, and a bipolar current is fainter than that for the positive polarity.

The leader stepping time, which is the pause time between steps, is required to create a new leader precursor and is strongly dependent on

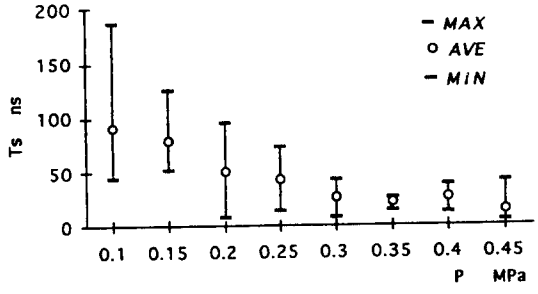

그림 12. 가스압력에 대한 리이더 스테핑 시간

Fig. 12. Leader stepping time plotted as a function of the gas pressure.

the gas pressure. Fig. 12 shows the relationship between the leader stepping time and the gas pressure in the positive polarity under the oscillating impulse voltage stress. The leader stepping time Ts is determined from the oscillogram of the prebreakdown current waveforms. The vertical lines and the circle marks indicate the variation range of the leader stepping time Ts and the average values, respectively. The leader stepping time Ts

decreases with increasing the gas pressure and its change is insignificant for gas pressure of more than 0.3 MPa.

Irregularity of the leader stepping time T_S is prominent for lower gas pressures and it exhibits a declining tendency as the gas pressure increases. It was observed that in the range of lower gas pressures, the streamer corona current is more intensive and the probability of direct breakdown which indicates a space charge controlled streamer breakdown is increased. Because the applied voltage is a damped oscillating impulse voltage, it is not obvious whether the fluctuation of the leader stepping time T_S is dominantly caused by the effect of corona space charges with a gas pressure or by the variation of applied voltage level. The leader propagation for a low gas pressure seems to be markedly influenced by the space charges effect due to streamer corona current level. The gas pressure increases accordingly, the attachment coefficient of SF_6 gas is increased and the radial development of the streamer corona sheath is reduced, the stepwise leader is frequently propagated.

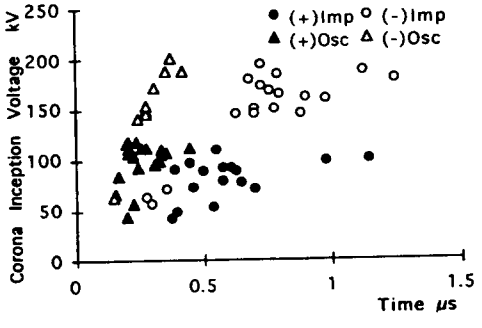

그림 13. 코로나 개시전압-시간관계

Fig. 13. Relation between corona inception voltage and time

The results of corona inception voltage under the non-oscillating and oscillating impulse voltages for a gas pressure of 0.3 MPa were shown in Fig. 13. The corona inception voltage then is determined by the appearance of the first corona current pulse as indicated in Fig. 10. The minimum corona inception voltages for the positive and negative polarities are approximately the same, but the deviation of corona inception voltage in the negative polarity is much more outstanding than that in the positive polarity. Also, it is known that the deviation of corona inception voltage is decreased with increasing the gas pressure.

In particular, the significant scatter of corona inception voltage in the negative polarity is appreciably associated with the cathode surface condition[14]. The microscopic protuberance protrudes on the surface of needle-shaped protrusion according as the electrical breakdown is repeated. Apparently, the field emission of initial electrons from the needle-shaped protrusion can be irregularly produced. As a consequence, the noticeable scatter of the breakdown voltages in the V-t characteristics and the corona inception voltages is believed to be due principally to statistical effect and other experimental uncertainties.

5. Conclusions

To obtain the information on the insulation level and breakdown mechanism of SF_6 gas caused by fast transient overvoltages, the dielectric behaviors and prebreakdown phenomena of SF_6 gas under non-oscillating and oscillating impulse voltages were investigated using a actual-sized GIS modeling apparatus. As a consequence, a single avalanche alone in inhomogeneous field contaminated by a conducting-particle is too weak to give rise to the electrical breakdown of the gas gap, and some other criteria such as the streamer to leader transition and the critical volume formation of space charges are necessary to bridge the test gap. The breakdown voltages of SF_6 gas in inhomogeneous field are noticeably influenced by the waveform and polarity of applied voltage and the emission mechanism of initial electrons. Comparing breakdown voltages in the presence of the positive polarity between the data for the non-oscillating and oscillating impulse voltages, there is little difference. However, it was found that the outstanding

difference between temporal prebreakdown developments for the non-oscillating and oscillating impulse voltages mainly results from the space charge effects. And bipolar prebreakdown currents were observed when the test gap was stressed by the oscillating impulse voltage.

※ This research was supported by the Institute for Science and Technology of Inha University in 1995

References

1. T. Kawamura, B.H. Lee, T. Nishimura and M. Ishii, "Dielectric Characteristics of SF_6 Gas under Steep-fronted Oscillating Impulse Voltages", Proc. of Conference of Discharge Research Group of IEEJ, pp.21~31, 1989.
2. T. Kawamura, B.H. Lee, T. Nishimura and M. Ishii, "Breakdown Characteristics of SF_6 Gap Disturbed by a Metallic Protrusion under Oscillating Transient Overvoltages", Jpn. J. Appl. Phys., Vol.33, No.4A, pp.2043~2049, 1994.
3. O. Farish, I.D. Chalmers, A. Gilbert and J. Dupuy, "The Streamer-Leader Transition in SF_6 and SF_6-Freon Mixtures", Porc. of 6th International Symposium on High Voltage Engineering(ISH), Paper No.32~03, 1989.
4. J.P. McGeehan, B.C. O'Neill, A.N. Prasad and J.D. Craggs, "Negative-ions/molecule reactions in sulphur hexafluoride", J. Phys., D., Vol.8, pp.153~161, 1975.
5. G. Riquel and Z.Y. Ren, "Insulating Behaviour of SF_6 Gaps Subjected to Fast Oscillating Overvoltages", Proc. of 9th Int, conf. on Gas Discharge, pp.331~334, 1988.
6. W. Shockley, "Currents to Conductors Induced by a Moving Point Charge", J. Appl. Phys., Vol. 9, pp. 635~636, 1938.
7. B. Gravendeel, et al, "External Discharge Currents in Inhomogeneous Field Configurations", J. Appl. Phys., Vol. 21, pp. 437~441, 1988.
8. Y.H. Paek, B.H. Lee and C.H. Ahn, "Development of the Sensor for Measuring the Electric Fields", T. of KIEE, Vol. 40, No. 6, pp. 630~637, 1991. 6.
9. B.H Lee, High-voltage and high current engineering, Cheongmungak Co., 1993, pp.42~45.
10. B.H. Lee and Y.H. Pack, "Prebreakdown Corona Processes of Point-to-Plane Gap in SF_6 Gas" J. KIEEME, Vol. 5, No.1, pp.99~110, 1992.
11. B.H. Lee, T. Kawamura and M. Ishii, "V-t Characteristics of SF_6 Gap Disturbed by a Needle-Shaped Protrusion under Oscillating Transient Overvoltages", T. of IEE of Japan, Vol.114-B, pp.664~669, 1994.
12. A. Heer and A. Stepkin, "Investigation on Discharge Development in SF_6 for Oscillating Lightning Impulse and Fast Oscillating Overvoltages", Proc. of 7th ISH, Paper No.31.06, 1991.
13. S. Matsumoto, H. Okubo, H. Aoyagi and S. Yanabu, "Non-uniform Flashover Mechanism in SF_6 Gas under Fast oscillating and Non-oscillating Impulse Voltages", Proc. of 6th ISH, Paper No.32.16, 1989.
14. B.H. Lee, C.H. Ahn, G.S. Kil and D.K. Jeon, "Breakdown Characteristics of Lightning Impulse and Oscillating Impulse Voltage under Non-uniform Field in SF_6 Gas", Trans. of KIEE, Vol.44, No.9, pp.1201-1207, 1995.

저자소개

이복희

1954년 6월 29일생. 1980년 인하대학교 공대 전기공학과 졸업. 1987년 동 대학원 전기공학과 졸업(박사). 1988년-89년 일본 동경대 생산기술연구소 객원연구원. 현재 인하대 공대 전기공학과 부교수.

이창준

1971년 5월 7일생. 1995년 인하대 공대 전기공학과 졸업. 현재 인하대 대학원 전기공학과 재학중(석사).

안창환

1959년 11월 4일생. 1983년 원광대 공대 전기공학과 졸업. 1991년 인하대 대학원 전기공학과 졸업(석사). 현재 인하대 대학원 전기공학과 박사과정.

전덕규

1962년 2월 9일생. 1995년 인하대 공대 전기공학과 졸업. 1993년 동 대학교 대학원 전기공학과 졸업(박사). 현재 서울산업대 자동차공학과 전임강사.

길경석

1962년 6월 30일생. 1984년 인하대 공대 전기공학과 졸업. 1996년 동 대학원 전기공학과 졸업(공박). 현재 한국해양대 이공대 전기공학과 전임강사.

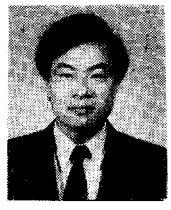

백승권

1955년 8월 26일생. 1979년 인하대 공대 전기공학과 졸업. 1981년 일본 게이오대학 졸업(박사). 현재 인제대 전기공학과 조교수